Charge-transfer salts of methylferrocenes with DCNQI derivatives (DCNQI = N,N′-dicyano-1,4-benzoquinonediimine): Crystal structures and magnetic properties

Funasako, Yusuke
Mochida, Tomoyuki
Sakurai, Takahiro
Ohta, Hitoshi

(Citation)
Journal of Organometallic Chemistry,696(13):2621-2626

(Issue Date)
2011-07

(Resource Type)
journal article

(Version)
Accepted Manuscript

(URL)
https://hdl.handle.net/20.500.14094/90001805

Charge-transfer salts of methylferrocenes with DCNQI derivatives (DCNQI = *N*,*N*′-dicyano-1,4-benzoquinonediimine): Crystal structures and magnetic properties

Yusuke Funasako[a], Tomoyuki Mochida[a,]*, Takahiro Sakurai,[b] Hitoshi Ohta[c]

[a]*Department of Chemistry, Graduate School of Science, Kobe University, Rokkodai, Nada, Hyogo 657-8501, Japan*

[b]*Center for Supports to Research and Education Activities, Kobe University, Rokkodai, Nada, Hyogo 657-8501, Japan*

[c]*Molecular Photoscience Research Center, Kobe University, Rokkodai, Nada, Hyogo 657-8501, Japan*

Abstract

Organometallic charge-transfer salts composed of decamethyl-, octamethyl-, and dimethylferrocene with *N*,*N*′-dicyano-1,4-benzoquinonediimine (DCNQI) derivatives were prepared. $[Fe(C_5Me_5)_2][(MeO)_2DCNQI]$ (**1**) and $[Fe(C_5Me_4H)_2][Me_2DCNQI]$ (**2**) were 1:1 DA salts with mixed-stack structures, whereas $[Fe(C_5Me_4H)_2][(MeO)_2DCNQI]_2$ (**3**) and $[Fe(C_5MeH_4)_2][DCNQI]_2$ (**4**) were 1:2 DA salts. **3** exhibited a segregated-stack structure, in which charge separation was observed in the acceptor column. **1** became a metamagnet below T_N = 5.0 K, whereas the other salts were paramagnets. Valence states and charge-transfer (CT) transitions in these complexes are discussed based on the neutral–ionic (NI) phase diagram.

Keywords: Crystal structures, Magnetic properties, Charge-transfer complex, Ferrocene, DCNQI

---

* Corresponding Author. Tel./fax: +81-78-803-5679

E-mail address: tmochida@platinum.kobe-u.ac.jp (T. Mochida)

1. Introduction

Metallocene-based charge-transfer (CT) complexes have attracted special attention because of their magnetic properties [1]. In particular, decamethylferrocene ([Fe(Cp*)$_2$]) has afforded a variety of CT complexes that are magnetically interesting [1, 2]. Among them, the most well-studied example is [Fe(Cp*)$_2$][TCNE] (TCNE = tetracyanoethylene), which exhibits ferromagnetic ordering below 4.8 K [3]. To date, many ferrocene-based CT complexes have been synthesized, such as those with TCNQ (= tetracyanoquinodimethane), metal-ditholates, and other anions [1–4]. In our studies, ferrocene-based CT complexes have been investigated in terms of valence states and phase transitions [5]. We recently prepared neutral metallocene complexes with quinone derivatives [6, 7] in search of neutral–ionic (NI) transitions in metallocene complexes. The NI transition is a transition from a high-temperature neutral state (D^0A^0) to a low-temperature ionic state (D^+A^-), characteristic of mixed-stack CT complexes that are located near the NI boundary [8]. We extended the NI phase diagram [7] and found that the NI boundary for ferrocene-based CT complexes is located where the difference between the redox potentials of the donor and acceptor ($\Delta E_{redox} = E_D - E_A$) is 0.095 V. In the present study, we used donors of [Fe(Cp*)$_2$] and [Fe(C$_5$Me$_4$H)$_2$] (= octamethylferrocene) and acceptors of DCNQI (= *N*,*N*′-dicyano-1,4-benzoquinonediimine) derivatives to search for complexes that are close to this region.

Here, we report the syntheses, magnetic properties, and crystal structures of a series of ferrocene–DCNQI complexes: [Fe(Cp*)$_2$][(MeO)$_2$DCNQI] (**1**), [Fe(C$_5$Me$_4$H)$_2$][Me$_2$DCNQI] (**2**), [Fe(C$_5$Me$_4$H)$_2$][(MeO)$_2$DCNQI]$_2$ (**3**), and [Fe(C$_5$MeH$_4$)$_2$][DCNQI]$_2$ (**4**) (Fig. 1). These are ionic complexes with ΔE_{redox} values close to the NI boundary. Related materials include a mixed-stack complex of [Fe(Cp*)$_2$][Me$_2$DCNQI] (**1′**), which is a metamagnet below T_N = 3.9 K [9], and a few other DCNQI-based metallocenium salts [10]. **1** showed metamagnetic behavior at low temperatures, similar to **1′**, whereas other salts were paramagnets.

2. Results and discussion

2.1. Syntheses and valence states

1–**3** were obtained as violet single crystals by recrystallization from acetonitrile or acetone, whereas **4** was

obtained as microcrystals. **1** and **2** exhibited a 1:1 DA ratio, whereas **3** and **4** exhibited 1:2 DA ratios. They were ionic complexes consisting of ferrocenium monocations. The average Fe–C(Cp) bond distances in the donors in **1**–**3**, determined crystallographically (vide infra), were 2.096 Å, 2.100 Å, and 2.096 Å, respectively, comparable to those in $[Fe(Cp^*)_2]^+$ and $[Fe(C_5Me_4H)_2]^+$ [11]. The degree of CT (ρ) on the acceptors was estimated using $\rho = A[c/(b + d)] + B$, similar to the case of TCNQ complexes [12]. In the equation, b, c, and d represent the bond lengths in the acceptors (Table 1), and the values of $A = -47.91$ and $B = 22.60$ were tentatively determined based on the geometries of the neutral and anionic forms of Me_2DCNQI [9]. As shown in Table 1, ρ was estimated to be −1 for the acceptors in **1** and **2**, and those for two crystallographically independent acceptors (A1 and A2) in **3** were −1 and 0, respectively.

The ρ values were also estimated from the C≡N stretching frequencies of the acceptors in the infrared spectra (Fig. S1), and the result was consistent with the estimation from the bond lengths. In **1** and **2**, the C≡N stretching vibration, observed at around 2176 cm^{-1} for neutral DCNQI molecules, shifted to lower energy by about 50 cm^{-1}, suggesting the value of $\rho \sim -1$. In **3**, two peaks corresponding to those of the neutral and monoanion species were observed at 2177 cm^{-1} and 2136 cm^{-1}, respectively. In **4**, the low energy shift was about 20 cm^{-1}, suggesting the value of $\rho \sim -0.5$, which is reasonable considering the 1:2 DA ratio.

To investigate CT absorption bands, UV-vis-NIR spectra of **1**–**4** and **1′** were measured. As shown in Fig. 2, all the salts exhibited broad absorption bands assignable to CT transitions at around 650–750 nm. The shapes of the CT bands for the 1:1 salts **1**, **2**, and **1′** are almost the same, accompanying a small peak around 800 nm. The band shapes for the 1:2 salts **3** and **4** differed from these. In Fig. 3, the CT energies in these salts are plotted against ΔE_{redox} (Table 2). Theoretical correlations between ΔE_{redox} and $h\nu_{CT}$ for ferrocene-based 1:1 DA complexes are shown as V-shaped lines [7]. Note that ΔE_{redox} (−0.10–0.07 V) of these salts are very close to the NI phase boundary (ΔE_{redox}= 0.095 V), and the plots are located near the apex of the theoretical lines. This is reasonable for **1**, **2**, and **1′** and validates our consideration of the theoretical correlation [7]. However, the 1:2 salts **3** and **4** should fall on a different ΔE_{redox}–$h\nu_{CT}$ correlation [7] if they have mixed-stack structures; thus, the result implies that they are not mixed-stack complexes. Consistently, **3** exhibited a segregated-stack structure (*vide infra*), whereas the structure of **4** is unknown. The absorption spectra in **3** likely include CT transitions between the acceptors.

An ionic mixed-stack complex located near the boundary might exhibit an “ionic-to-neutral” transition at high temperatures, which should accompany paramagnetic–diamagnetic changes. However, no such transitions were found in **1**–**4** by SQUID measurements. No phase transitions could be detected for **1**–**4** and **1′** by DSC (differential scanning calorimetry) measurements between 100–373 K. In terms of $\Delta E_{\mathrm{redox}}$, octamethylferrocene complex **2** was located nearer to the NI transition than decamethylferrocene complex **1'**, but an NI transition is less likely to occur in **2** because of its much smaller cell volume compared with **1'** (*vide infra*). We also tried other combinations that fall on the NI boundary using donors of octamethylformyl-, dimethyl-, and non-substituted-ferrocene and acceptors of MeO_2-, Me_2-, and non-substituted-DCNQI. However, no complexes were obtained except for **1**–**4**; in particular, the combinations that might afford neutral complexes were difficult to form. Among the obtained salts, the combination for **3** was the closest to the NI boundary in terms of redox potential, although it did not give a 1:1 mixed-stack structure suitable for an NI transition.

*2.2 Crystal structures of **1** and **2***

Packing diagrams of **1** and **2** are shown in Figs. 4 and 5, respectively. Both crystals belong to the space group of $P\bar{1}$. The donors and acceptors are stacked alternately in both crystals, and their assembled structures closely resemble that of **1′** [9]. In **1**, there is one crystallographically independent donor molecule and two centrosymmetric acceptor molecules. The Cp* rings in the cation are in a nearly eclipsed conformation. In **2**, both the donor and the acceptor are centrosymmetric, and the donor exhibited a staggered conformation of the C_5 rings. In the unit cell, there are three distinct chains, as shown in the figures, displaying three unique interchain arrangements, similar to the case of **1′** [9]. The arrangements of I–II and II–III are out-of-registry and that of I–III is in-registry.

Intermolecular distances and interchain distances in **1**, **2**, and **1'** are listed in Table 3. The intrachain Fe···Fe distances and intrachain Cp...acceptor centroid distances in **2** are slightly shorter than those in **1** and **1'**. Similarly, the interchain separation of II–III is significantly shorter in **2**, which corresponds to the lack of methyl groups in **2**. Separation of I–II is significantly longer in **1** due to the replacement of the methyl group by the methoxy group. The molecular volumes of **1** and **1′** in the crystals are comparable, despite the presence

of two more oxygen atoms in **1**, considering the unit cell volumes (**1**: 1354.5 Å^3 at −173 °C, Z = 2; **1′**: 676.14 Å^3 at 25 °C, Z = 1). The unit cell volume of octamethylferrocene complex **2** (601.7 Å^3, at −173 °C) is about 10% smaller than that of decamethylferrocene complex **1'** (676.14 Å^3, at 25 °C).

*2.3 Magnetic properties of **1** and **2***

The temperature dependence of the magnetic susceptibilities for **1** and **2** are shown in Fig. 6. The observed χT value of 1.2 emu K mol^{-1} at room temperature agrees reasonably with the sum of the values for $[Fe(Cp^*)_2]^+$ and the DCNQI anion [9]. In **1**, the χT value increased with decreasing temperature, indicating the presence of ferromagnetic interactions. The magnetic susceptibility in this temperature range obeyed the Curie–Weiss law [$\chi = C/(T - \theta)$] with θ = 7.0 K. Further cooling led to the antiferromagnetic transition at T_N = 5.0 K, which accompanied an abrupt drop in the χT value. The magnetization curve measured at 1.8 K is plotted in the inset of Fig. 6. A sigmoidal curve characteristic of a metamagnet was observed, exhibiting an inflection point around H_C = 0.24 T. In contrast, only paramagnetic behavior was observed for **2** down to 2 K. The magnetic susceptibility followed the Curie–Weiss law, with θ = −3.17 K, whereas the decrease in χT below 20 K is ascribed to the reduction of the orbital contribution from the donor.

The magnetic behavior of **1** is similar to that of **1′** [9]. At high temperatures, the magnetic behavior is dominated by ferromagnetic interchain interactions, whereas it exhibits antiferromagnetic behavior below T_N due to antiferromagnetic intrachain interactions. Comparison of the magnetic parameters in **1** (θ = 7.0 K, T_N = 5.0 K, and H_c = 0.24 T) and **1′** (θ = 3.0 K, T_N = 3.9 K, and H_c = 0.55 T [9]) demonstrates that θ and T_N are larger in **1**. This is accounted for by the shorter D–A intrachain separations in **1**; the centroid distances between the Cp and C_6 rings of the acceptor in **1** are 3.576 Å and 3.598 Å, whereas that in **1′** is 3.618 Å (Table 3). Consistently, the Fe...Fe intrachain distances are shorter in **1**. Indeed, shorter intrachain DA separation is known to give larger values of θ, as discussed for relevant salts [9], and T_N is proportional to $|E_{intra}E_{inter}|^{1/2}$, where E_{inter} is an effective interchain interaction, and E_{intra} is proportional to DA intrachain magnetic coupling. On the other hand, H_C correlates to the strength of the antiferromagnetic interactions. In **1′**, the most magnetically significant interchain contact is between the nitrogen atoms of the acceptors (N...N distance: 3.939 Å) [9], whereas there are no such intermolecular contacts in **1**, which may account for its smaller H_c.

Overall, the magnetic parameters for **1** are consistent with the crystal structure.

Despite the slightly shorter intrachain DA distances and interchain distances in **2** compared with those in **1** and **1′,** as described above (Table 3), magnetic order or ferromagnetic interactions were absent in **2**. This is most like attributable to the lower symmetry of $[Fe(C_5Me_4H)_2]^+$, leading to the absence of ferromagnetic interactions, as has been discussed for the TCNQ salts [13]. Indeed, for $[Fe(Cp^*)_2][TCNQ]$ and $[Fe(C_5Me_4H)_2][TCNQ]$, only the former exhibits metamagnetic behavior [13, 14].

*2.4 Crystal structure of **3***

The packing diagram of **3** is shown in Fig. 7. The crystal belongs to the space group *P*–1. The donors and acceptors are stacked along the *a*-axis, forming a segregated-stack structure. The donor is centrosymmetric, displaying a staggered conformation of the C_5 rings. Two crystallographically independent centrosymmetric acceptor molecules, denoted as A1 and A2 (Fig. 7), are stacked alternately with a regular interval of 3.837 Å (centroid–centroid distance). As shown above, A1 and A2 are monoanion and neutral molecules, respectively, displaying complete charge separation in the column. As seen in Fig. 7, A1 is close to the Fe atom of the cation, and, hence, localization of the negative charge on this molecule is reasonably attributed to the cation–anion electrostatic interactions.

*2.5 Magnetic properties of **3** and **4***

The temperature dependence of the magnetic susceptibilities of **3** and **4** is shown in Fig. 8. These complexes were paramagnets in the measured temperature range. The χT value for **3** was 1.2 emu K mol^{-1} at room temperature, in good agreement with the sum of the values for $[Fe(Cp^*)_2]^+$ and DCNQI anion. The value gradually decreased with decreasing temperature. Considering the regular one-dimensional anion arrangement, the temperature dependence was tentatively fitted by applying the Bonner–Fisher model [15] to the acceptor spins, taking into account the contribution of the donor spins and temperature-independent paramagnetism (TIP). The fitting afforded an antiferromagnetic interaction of $|J|/k_B \approx -60$ K between the anions and TIP of 2 × 10 emu·mol^{-1}. The decrease of χT below 20 K is ascribed to the reduction of the orbital contribution from the donor.

The χT value for **4** was 0.66 emu K mol^{-1} at room temperature, corresponding to the value of the ferrocenium cation only. It is unlikely that the contribution from the acceptor spins disappears in a mixed-stack complex. Hence, the complex probably has a segregated-stacked structure, in which the acceptors may form tetramers in the column, which is likely to be diamagnetic. This is consistent with the discussion given above on the CT bands in **4**.

3. Conclusion

In search of possible NI transitions in metallocenium salts, we prepared several ferrocenium salts with DCNQI anions. [Fe(Cp*)$_2$][(MeO)$_2$DCNQI] (**1**) and [Fe(C$_5$Me$_4$H)$_2$][Me$_2$DCNQI] (**2**) formed typical 1:1 DA salts with mixed-stack structures, of which **1** exhibited a ferromagnetic intrachain interaction (θ = 7.0 K) and metamagnet behavior below T_N = 5.0 K. Only the decamethylferrocenium salt showed significant magnetic interactions, similar to [Fe(Cp*)$_2$][TCNQ] and [Fe(C$_5$Me$_4$H)$_2$][TCNQ]. The magnetic interaction in **1** was larger than that in [Fe(Cp*)$_2$][Me$_2$DCNQI] (θ = 3.0 K and T_N = 3.9 K), and this is ascribable to shorter D–A intrachain separations. Although **1** and **2** are located near the NI boundary, no NI transition was observed up to 373 K. Among the obtained salts, the redox potential of [Fe(C$_5$Me$_4$H)$_2$][(MeO)$_2$DCNQI]$_2$ (**3**) was the closest to the NI boundary, although the salt exhibited a segregated-stack structure with a 1:2 DA ratio, which is unsuitable for NI transitions. We also tried other combinations of methylferrocenes and TCNQ or DCNQI derivatives that fall on the NI boundary, but no crystalline complexes were obtained except for the present salts. Further investigation is needed to construct organometallic CT complexes located closer to the NI boundary.

4. Experimental

4.1 Materials and physical measurements

Me$_2$DCNQI, (MeO)$_2$DCNQI, and [Fe(Cp*)$_2$][Me$_2$DCNQI] (**1′**) were prepared according to the literature [9,16]. Other chemicals were commercially available. Infrared spectra were recorded as KBr pellets on a Thermo Nicolet Avatar 360 spectrometer. Solid-state electronic absorption spectra were measured on a JASCO V-570 UV/VIS/NIR spectrometer. DSC measurements were performed for **1**–**4** and **1′** using a Q100

differential scanning calorimeter (TA instruments) in the temperature range of 100–373 K at a rate of 10 $K \cdot min^{-1}$. Elemental analyses were performed with a Yanaco CHN coder MT5. Magnetic susceptibilities were measured using a Quantum Design MPMS-XL5 SQUID susceptometer under a magnetic field of 0.1 T. The temperature range was 2–300 K for **1**, **3**, and **4** and 2–370 K for **2**. Compressed polycrystalline samples were used to minimize orientation effects.

4.2 Syntheses

4.2.1 Preparation of [Fe(Cp)$_2$][(MeO)$_2$DCNQI] (**1**)*

[Fe(Cp*)$_2$] (60 mg, 0.19 mmol) and (MeO)$_2$DCNQI (40 mg, 0.19 mmol) were dissolved in acetonitrile, and the saturated solution was allowed to cool to −40 °C over several days. The precipitated crystals were collected by filtration and dried in vacuo; violet plates were obtained in a yield of 90.8 mg (91%). The crystals were suitable for X-ray structure determination. Anal. calcd. for $C_{30}H_{38}FeN_4O_2$ (542.49): C, 66.42; H, 7.06; N, 10.33. Found: C, 66.46; H, 7.02; N, 10.42.

*4.2.2 Preparation of [Fe(C$_5$Me$_4$H)$_2$][Me$_2$DCNQI] (**2**)*

[Fe(C_5Me_4H)$_2$] (80 mg, 0.27 mmol) and Me$_2$DCNQI (50 mg、0.27 mmol) were dissolved in 20 mL of acetone, and the solvent was allowed to evaporate at room temperature. Violet microcrystals were obtained at a yield of 120.8 mg (92%). Block crystals suitable for X-ray structure determination were obtained by slow evaporation of an acetone solution at −16 °C.

*4.2.3 Preparation of [Fe(C$_5$Me$_4$H)$_2$][(MeO)$_2$DCNQI]$_2$ (**3**)*

[Fe(C_5Me_4H)$_2$] (100 mg, 0.34 mmol) and (MeO)$_2$DCNQI (69 mg, 0.32 mmol) were dissolved in acetonitrile, and the saturated solution was allowed to cool to –40 °C over several days. Precipitated crystals were collected by filtration, washed with hexane to remove excess [Fe(C_5Me_4H)$_2$], and dried in vacuo. Violet block crystals were obtained in a yield of 91.0 mg (76%). The obtained crystals were suitable for X-ray structure determination. Anal. Calcd.for $C_{38}H_{42}FeN_8O_4$ (730.64): C, 62.47; H, 5.79; N, 15.34. Found: C, 62.35; H, 5.69; N, 15.44.

*4.2.4 Preparation of [Fe(C_5MeH_4)$_2$][DCNQI]$_2$ (**4**)*

[Fe(C_5MeH_4)$_2$] (54.8 mg, 0.26 mmol) and DCNQI (40 mg, 0.26 mmol) were dissolved in dichloromethane, and the saturated solution was allowed to cool to −40 °C over several days. Precipitated crystals were collected by filtration and dried in vacuo. Dark green needle crystals were obtained in a yield of 23.6 mg (70%). The crystals were suitable for X-ray structure determination. Anal. Calcd. for $C_{28}H_{22}FeN_8$ (526.37): C, 63.89; H, 4.21; N, 21.29. Found: C, 62.59; H, 4.18; N, 21.21.

4.3 X-ray structure determination

X-ray diffraction data for single crystals were collected on a Bruker SMART APEX II Ultra CCD diffractometer using Mo Kα radiation (λ = 0.71073 Å). Crystal data, data collection parameters, and analysis statistics for these compounds are listed in Table 4. All calculations were performed using SHELXL [17]. The non-hydrogen atoms were refined anisotropically, and hydrogen atoms were inserted at calculated positions. Empirical absorption corrections (SADABS) [18] were applied. The packing diagrams were drawn using ORTEP-3 [19]. CCDC 791709 (**1**), 809046 (**2**), and 809047 (**3**) contain the supplementary crystallographic data for this paper.

Acknowledgments

This work was financially supported by KAKENHI. We thank Y. Furuie (Kobe University) for elemental analysis and M. Nakama (WarpStream Ltd., Tokyo) for providing Web-based database systems.

Appendix A. Supplementary material

Infrared spectra of **1**–**4** (Fig. S1) and crystallographic CIF files for **1**–**3**. Supplementary data related to this article can be found online, at doi:10.1016/j.jorganchem.XXXX.XX.XXX.

References

[1] (a) A. Togni, T. Hayashi (Eds.), Ferrocenes: Homogenous Catalysis, Organic Synthesis, Materials Science,

Wiley–VCH: Weinheim, 1995, Chapter 8, and references therein; (b) J. S Miller, M. Drillon (Eds.), Magnetism: molecules to materials V, Wiley–VCH: Weinheim, 2005. Chapters 1 and 7, and references therein; (c) D. de Caro, C. Faulmann, L. Valade, Chem. Eur. J. 13 (2007) 1650–1663.

[2] (a) J.S. Miller, J. Mater. Chem. 20 (2010) 1846–1857; (b) V. Gama, M. Almeida, Top. Organomet. Chem. 27 (2009) 97–140.

[3] J.S. Miller, J. C. Calabrese, H. Rommelmann, S.R. Chittipeddi, J.H. Zhang, W.M. Reiff, A.J. Epstein, J. Am. Chem. Soc. 109 (1987) 769–781.

[4] (a) D. Bellamy, N.G. Connelly, G.R. Lewis A.G. Orpen, CrystEngComm 4 (2002) 51–58; (b) M. Fettouhi, L. Ouahab, M. Hagiwara, E. Codjovi, O. Kahn, H. Constant-Machado, F. Varret, Inorg. Chem. 34 (1995) 4152–4159.

[5] (a) T. Mochida, T. Koinuma, T. Akasaka, M. Sato, Y. Nishio, K. Kajita, H. Mori, Chem. Eur. J. 13 (2007) 1872–1881; (b) T. Mochida, K. Takazawa, H. Matsui, M. Takahashi, M. Takeda, M. Sato, Y. Nishio, K. Kajita, H. Mori, Inorg. Chem. 44 (2005) 8628–8641; (c) T. Mochida, K. Takazawa, M. Takahashi, M. Takeda, Y. Nishio, M. Sato, K. Kajita, H. Mori, M.M. Matsushita, T. Sugawara, J. Phys. Soc. Jpn., 74 (2005) 2214–2216.

[6] (a) H. Nakamura, D. Kuwahara, T. Mochida, J. Phys. Chem. A, 113 (2009) 13601–13607; (b) T. Mochida, K. Yoza, J. Organomet. Chem. 695 (2010) 1749–1752.

[7] T. Mochida, Y. Funasako, H. Azumi, submitted.

[8] J.B. Torrance, J.E. Vazquez, J.J. Mayerle, V.Y. Lee, Phys. Rev. Lett. 46 (1981) 253–257.

[9] S. Rabaça, R. Meira, L.C.J. Pereira, M. Teresa Duarte, V. da Gama, J. Organomet. Chem. 632 (2001) 67–74.

[10] (a) J.S. Miller, C. Vazquez, R.S. McLean, W.M. Reiff, A. Aumüller, S. Hunig, Adv. Mater. 5 (1993) 448–450; (b) S. Rabaça, R. Meira, J. Soares, M.T. Duarte, V. Gama, Synth. Met. 121 (2001) 1828–1829.

[11] (a) A. S. Perucha, M. Bolte, Acta Cryst. E63 (2007) m1703; (b) V.G. Andrianov, Y.T. Struchkov, I.R. Lyatifov, R.B. Materikova, Koord. Khim. 8 (1982) 846–850.

[12] T.J. Kistenmacher, T.J. Emge, A.N. Bloch, D.O. Cowan, Acta Cryst. B38 (1982) 1193–1199.

[13] J.S. Miller, D.T. Glatzhofer, D.M. O'Hare, W.M. Reiff, A. Chakraborty, A.J. Epstein, Inorg. Chem. 28 (1989) 2930–2939.

[14] J.S. Miller, J.H. Zhang, W.M. Reiff, D.A. Dixon, L.D. Preston, A.H. Reis, E. Gebert, M. Extine, J. Troup, A.J. Epstein, M.D. Ward, J. Phys. Chem. 91 (1987) 4344–4360.

[15] W.E. Hatfield, R.R. Weller, J.W. Hall, Inorg. Chem. 19 (1980) 3825–3828.

[16] A. Aumüller, S. Hünig, Liebigs Ann. Chem. (1986) 142–164.

[17] G.M. Sheldrick, SHELXL: Program for the Solution for Crystal Structures, University of Göttingen, Germany, 1997.

[18] G.M. Sheldrick, SADABS: Program for Semi-empirical Absorption Correction, University of Göttingen, Germany, 1997.

[19] L.J. Farrugia, ORTEP-3 for Windows, J. Appl. Cryst. 30 (1997) 565–566.

[20] A. Aumüller, P. Erk, S. Hünig, E. Hädicke, K. Peters, H. G. V. Schnering, Chem. Ber. 124 (1991) 2001–2004.

[21] S. Fukuzumi, H. Kotani, T. Suenobu, S. Hong, Y. -M. Lee, W. Nam, Chem. Eur. J.16 (2010) 354–361.

[22] A. Aumüller, S. Hünig, Liebigs Ann. Chem. (1986) 165–176.

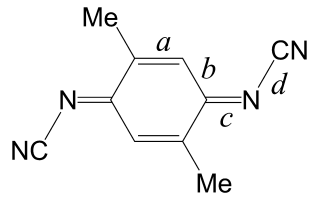

Chart 1.

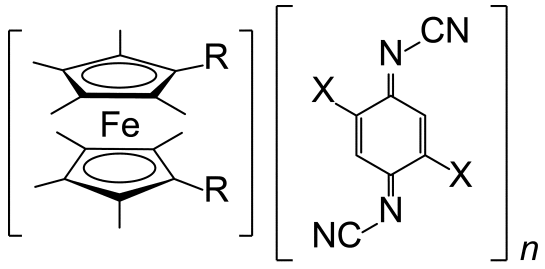

1: R = Me, X = OMe (*n* = 1)
2: R = H, X = Me (*n* = 1)
3: R = H, X = OMe (*n* = 2)

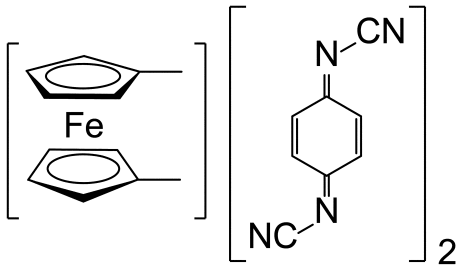

4

Fig. 1. Chemical formulas of **1**–**4**.

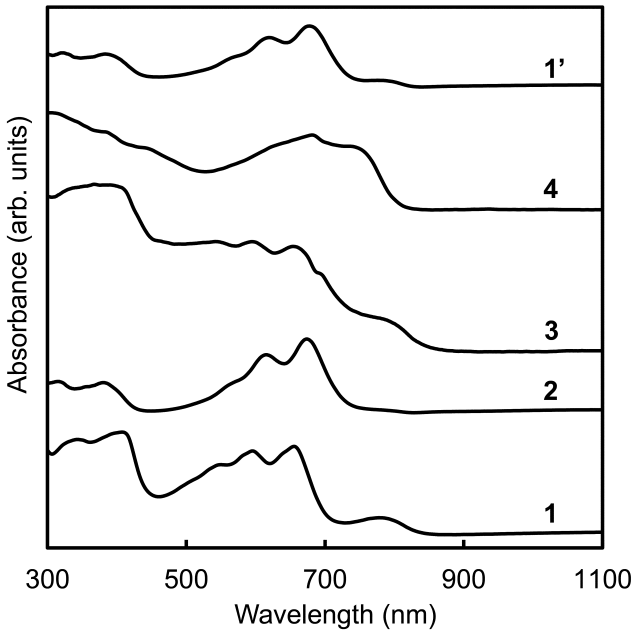

Fig. 2. UV-vis-NIR spectra of $[Fe(Cp^*)_2][(MeO)_2DCNQI]$ (**1**), $[Fe(C_5Me_4H)_2][Me_2DCNQI]$ (**2**), $[Fe(C_5Me_4H)_2][(MeO)_2DCNQI]_2$ (**3**), $[Fe(C_5MeH_4)_2][DCNQI]_2$ (**4**), and $[Fe(Cp^*)_2][Me_2DCNQI]$ (**1′**).

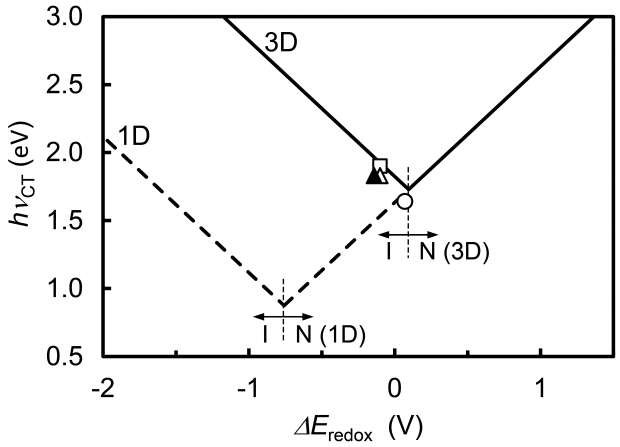

Fig. 3. Correlations between ΔE_{redox} and CT transition energies in ferrocene-based CT complexes. Theoretical correlations for 1:1 DA complexes with 3D and 1D interactions are represented by solid lines and dotted lines, respectively, and the apices of the lines correspond to the neutral–ionic boundary. Plots for $[Fe(Cp^*)_2][(MeO)_2DCNQI]$ (**1**; □), $[Fe(C_5Me_4H)_2][Me_2DCNQI]$ (**2**; Δ), $[Fe(C_5MeH_4)_2][DCNQI]_2$ (**4**; ○), and $[Fe(Cp^*)_2][Me_2DCNQI]$ (**1′**; ▲) are shown.

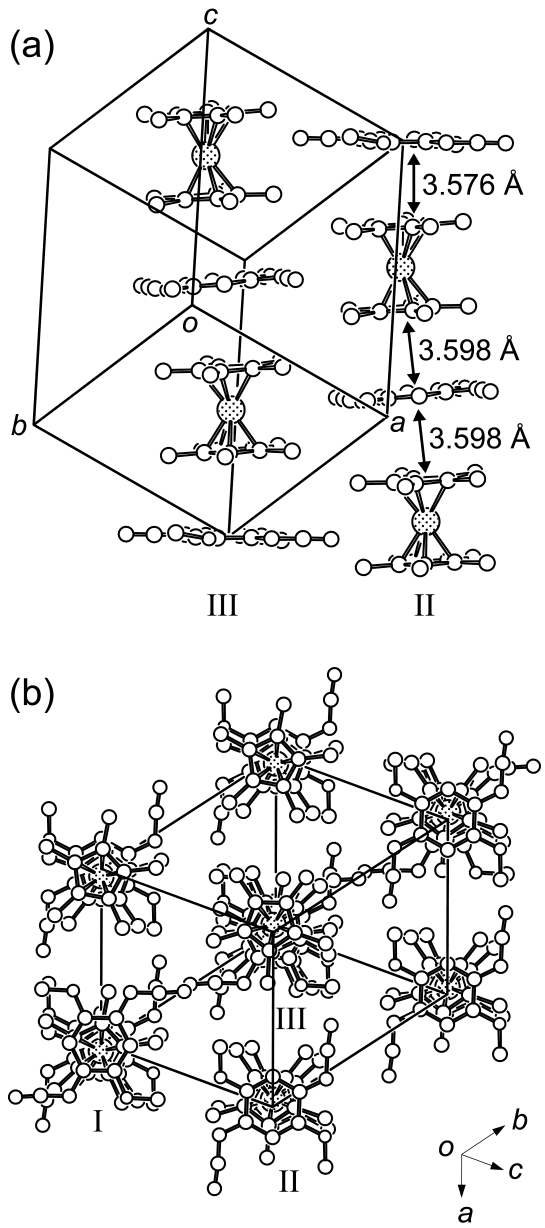

Fig. 4. Packing diagrams of **1**, projected (a) normal to the stacking direction and (b) along the stacking direction. Hydrogen atoms are omitted for clarity.

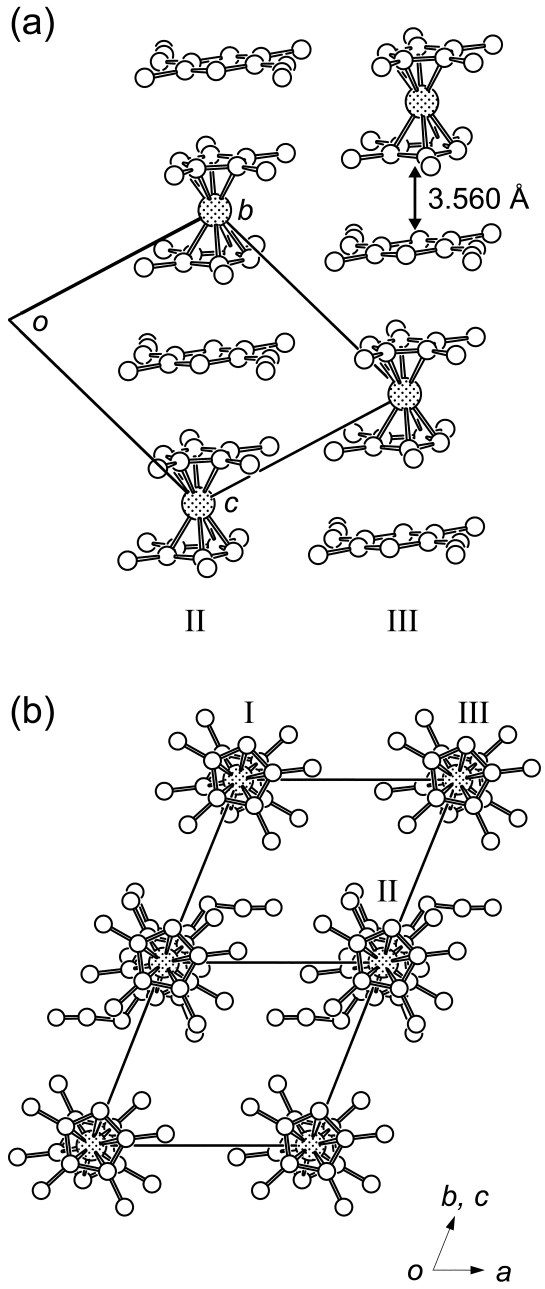

Fig. 5. Packing diagrams of **2**, projected (a) normal to the stacking direction and (b) along the stacking direction. Hydrogen atoms are omitted for clarity.

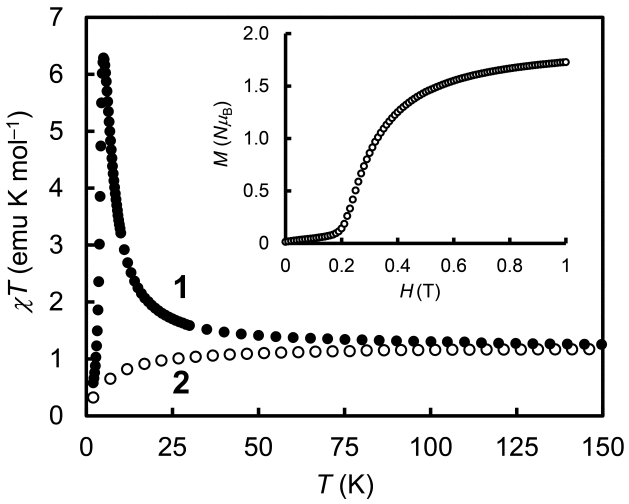

Fig. 6. Temperature dependence of the magnetic susceptibilities of **1** (●) and **2** (○) presented as χT versus T. The inset shows the magnetization curve for **1** at 1.8 K.

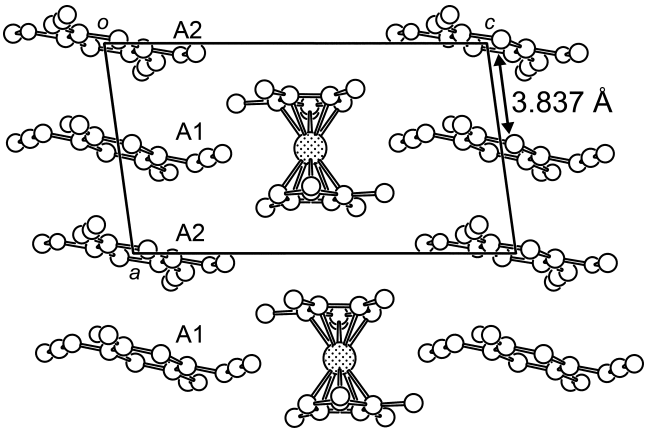

Fig. 7. Packing diagrams of **3** projected along the *b*-axis. Hydrogen atoms are omitted for clarity.

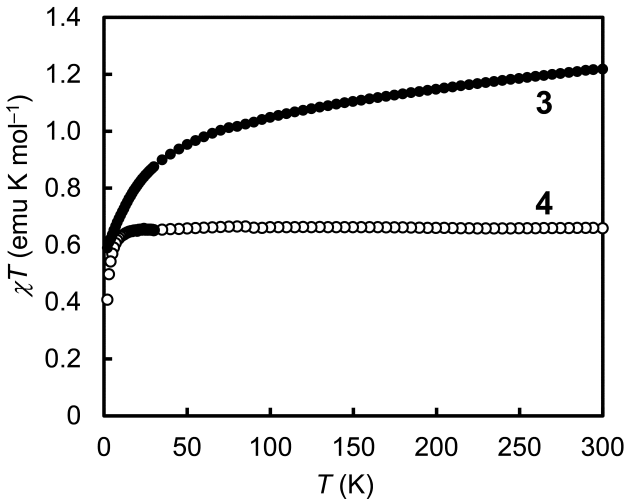

Fig. 8. Temperature dependence of the magnetic susceptibilities of **3** (●) and **4** (○) presented as χT versus T.

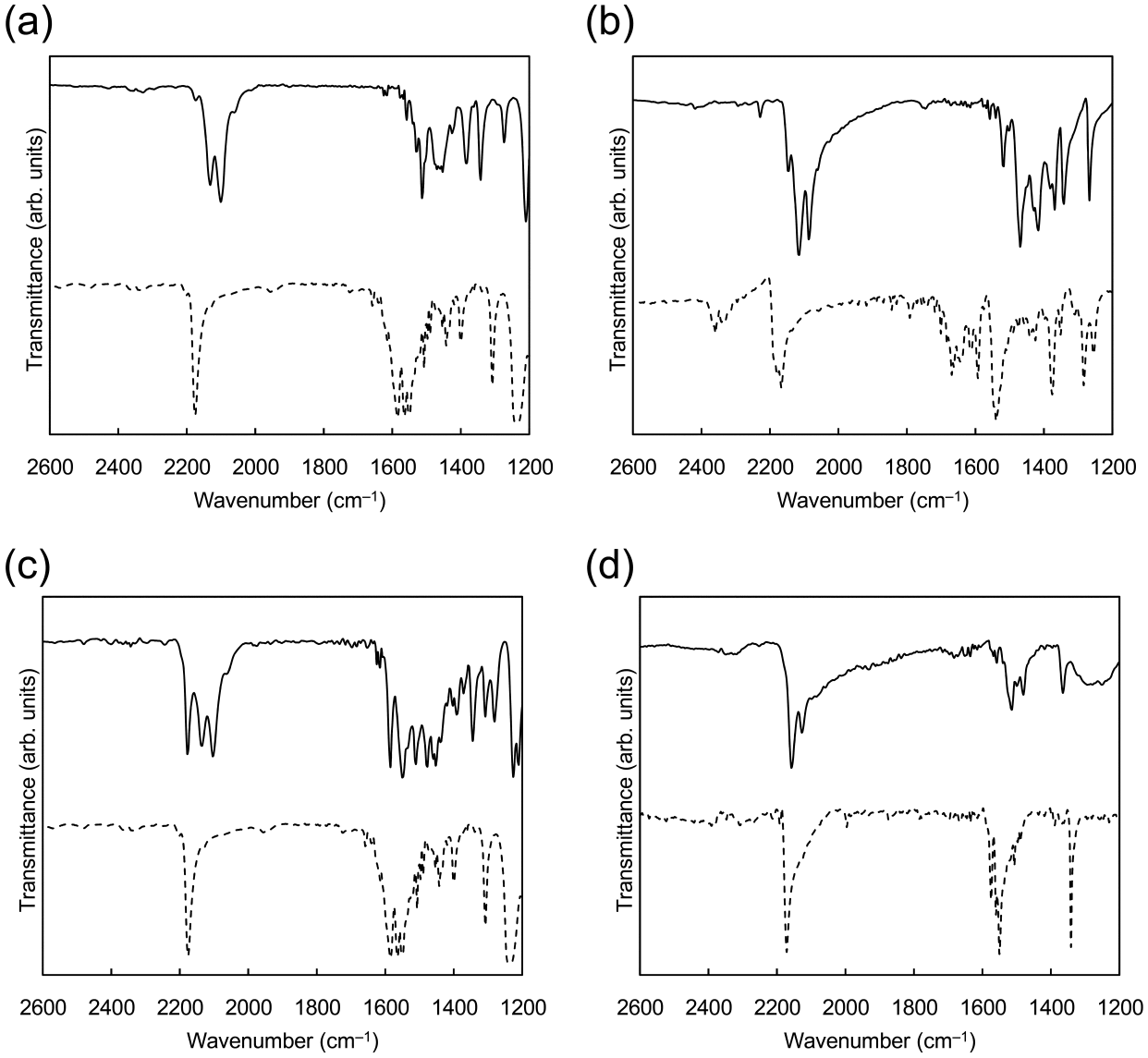
(a)
(b)
(c)
(d)
Transmittance (arb. units)
Wavenumber (cm⁻¹)
2600 2400 2200 2000 1800 1600 1400 1200

Fig. S1

Table 1

Selected bond lengths[a] and the degree of charge-transfer (ρ) on the acceptors in **1**–**3** and reference compounds.

Compounds		a (Å)	b (Å)	c (Å)	d (Å)	$c/(b + d)$ (Å)	ρ [b]
$[Fe(Cp^*)_2][(MeO)_2DCNQI]$ (**1**)		1.365	1.419	1.352	1.321	0.494	−1.0
$[Fe(C_5Me_4H)_2][Me_2DCNQI]$ (**2**)		1.368	1.429	1.354	1.325	0.492	−1.0
$[Fe(C_5Me_4H)_2][(MeO)_2DCNQI]_2$ (**3**)	(A1)	1.372	1.416	1.352	1.320	0.494	−1.1
	(A2)	1.350	1.436	1.306	1.339	0.471	0.0
Me_2DCNQI[c, d]		1.341	1.447	1.319	1.350	0.472	0.0
$[Fe(Cp^*)_2][Me_2DCNQI]$ (**1'**)[c, e]		1.366	1.425	1.352	1.320	0.493	−1.0

[a]Definition of a–d are shown in Chart 1.

[b]$\rho = A[c/(b + d)] + B$ with $A = -47.91$ and $B = 22.60$.

[c]Reference compounds. [d]ref. 20. [e]ref. 9.

Table 2

Redox potentials of the components of ferrocene-based CT complexes and their CT energies.

Compounds	E_D (V)[a]	E_A (V)[a]	ΔE_{redox} (V)[b]	$h\nu_{CT}$ (eV)
$[Fe(Cp^*)_2][(MeO)_2DCNQI]$ (**1**)	−0.08[d]	0.02[e, f]	−0.10	1.90
$[Fe(C_5Me_4H)_2][Me_2DCNQI]$ (**2**)	−0.04[d]	0.06[e, f]	−0.10	1.83
$[Fe(C_5Me_4H)_2][(MeO)_2DCNQI]_2$ (**3**)	−0.08	0.06	−0.14	1.83
$[Fe(C_5MeH_4)_2][DCNQI]_2$ (**4**)	0.26[d]	0.19[e, f]	0.07	1.64
$[Fe(Cp^*)_2][Me_2DCNQI]$ (**1'**)[c]	0.26	0.19	0.07	1.64

[a]Half-wave redox potentials of donors (E_D) and acceptors (E_A) vs. SCE.

[b]ΔE_{redox} / V = $E_D - E_A$.

[c]ref. 9.

[d]ref. 21.

[e]ref. 22.

[f]Potentials referenced to SCE.

Table 3
Intermolecular and interchain distances in **1**, **2**, and **1'**.

Compounds	Fe···Fe[a] (Å)	Cp···C_6[b] (Å)	I–II (Å)	II–III (Å)	I–III (Å)
$[Fe(Cp^*)_2][(MeO)_2DCNQI]$ (**1**)	10.535, 10.603	3.576, 3.598	9.528	8.057	8.456
$[Fe(C_5Me_4H)_2][Me_2DCNQI]$ (**2**)	10.511	3.560	8.840	7.461	8.264
$[Fe(Cp^*)_2][Me_2DCNQI]$ (**1'**)[c]	10.641	3.617	8.860	8.373	8.486

[a]Intrachain distances.

[b]Donor–acceptor distances (centroids of Cp and C_6 rings).

[c]ref. 9.

Table 4
Crystallographic parameters for **1**, **2**, and **3**.

	1	**2**	**3**
Empirical formula	C_{30} H_{38} Fe N_4 O_2	C_{28} H_{34} Fe N_4	C_{38} H_{42} Fe N_8 O_4
Formula weight (g mol^{-1})	542.49	482.44	730.65
Crystal system	Triclinic	Triclinic	Triclinic
Space group	$P\bar{1}$	$P\bar{1}$	$P\bar{1}$
a (Å)	9.448(3)	8.531(5)	7.6740(12)
b (Å)	10.578(3)	8.996(5)	8.7977(14)
c (Å)	14.330(4)	9.260(5)	13.853(2)
α (°)	91.693(4)	70.289(5)	75.843(2)
β (°)	104.659(4)	81.783(5)	79.089(2)
γ (°)	101.203(3)	64.072(5)	75.608(2)
Volume ($Å^3$)	1354.5(6)	601.7(6)	870.1(2)
Z	2	1	1
$d_{calcd.}$ (g cm^{-3})	1.330	1.331	1.394
μ (mm^{-1})	0.591	0.650	0.487
Reflections collected	6597	2699	4145
Independent reflections	4842 (R_{int} = 1.97%)	1951 (R_{int} = 1.95%)	3016 (R_{int} = 1.26%)
$F(000)$	576	256	384
R_1[a)], wR_2[b)] ($I > 2\sigma(I)$)	0.0368, 0.0772	0.0339, 0.0954	0.0276, 0.0773
R_1[a], wR_2[b] (all data)	0.0505, 0.0832	0.0342, 0.0957	0.0281, 0.0736
Goodness-of-fit on F^2	1.021	1.076	1.071
Completeness to θ (%)	97.5	98.4	98.1
Parameters	346	156	238
Largest diff. peak and hole (e $Å^{-3}$)	0.339 and −0.268	0.767 and −0.409	0.277 and −0.304

[a]$R_1 = \Sigma \, ||F_o| - |F_c|| \, / \, \Sigma \, |F_o|$.

[b]$wR_2 = [\, \Sigma \, w(F_o^2 - F_c^2)^2 \, / \, \Sigma \, w(F_o^2)^2 \,]^{1/2}$.

TOC